Environmental Science & Technology

Characterization of Natural and Affected Environments

Plutonium desorption from nuclear melt glass-derived colloids and implications for migration at the Nevada National Security Site, USA

Claudia Joseph, Enrica Balboni, Teresa Marie Baumer, Kerri Treinen, Annie B. Kersting, and Mavrik Zavarin

Environ. Sci. Technol., **Just Accepted Manuscript** • DOI: 10.1021/acs.est.9b03956 • Publication Date (Web): 07 Oct 2019

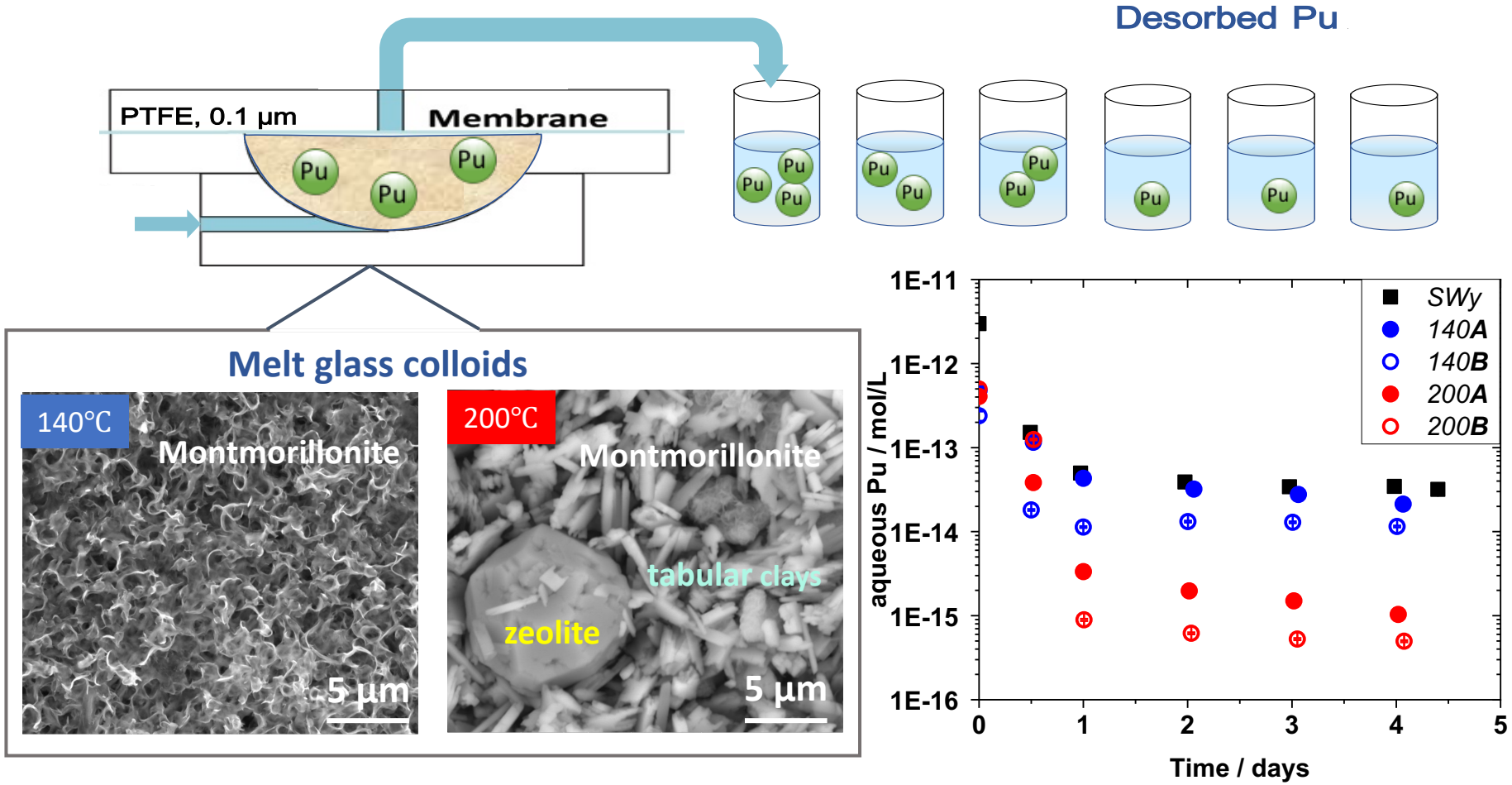
PTFE, 0.1 µm
Membrane
Pu
Desorbed Pu
Melt glass colloids
140°C
Montmorillonite
5 µm
200°C
Montmorillonite
tabular clays
zeolite
5 µm
SWy
140A
140B
200A
200B
aqueous Pu / mol/L
1E-11
1E-12
1E-13
1E-14
1E-15
1E-16
0
1
2
3
4
5
Time / days

LLNL-JRNL-764142

Plutonium desorption from nuclear melt glass-derived colloids and implications for migration at the Nevada National Security Site, USA

Claudia Joseph[ab†], Enrica Balboni[a†*], Teresa Baumer[c], Kerri Treinen[a], Annie B. Kersting[a], Mavrik Zavarin[a]

[a] Glenn T. Seaborg Institute, Physical & Life Sciences Directorate, Lawrence Livermore National Laboratory, L-231, P.O. Box 808, Livermore, CA 94550, USA.

[b] Current address: Karlsruhe Institute of Technology, Institute for Nuclear Waste Disposal (INE), Hermann-von-Helmholtz-Platz 1, 76344 Eggenstein-Leopoldshafen, Germany.

[c] Department of Civil & Environmental Engineering & Earth Sciences, University of Notre Dame, Notre Dame, IN 46556, USA.

[†] These authors contributed equally to the manuscript.

[*] Corresponding author email: balboni1@llnl.gov; phone: (925)-422-4833.

LLNL-JRNL-764142

Abstract

The migration of low levels of plutonium has been observed at the Nevada National Security Site (NNSS) and attributed to colloids. To better understand the mechanism(s) of colloid-facilitated transport at this site, we performed flow cell desorption experiments with mineral colloid suspensions produced by hydrothermal alteration of NNSS nuclear melt glass, residual material left behind from nuclear testing. Three different colloid suspensions were used, 1) colloidal material from hydrothermal alteration of nuclear melt glass at 140 °C, 2) at 200 °C, and 3) plutonium sorbed to SWy-1 montmorillonite at room temperature. The 140 °C sample contained only montmorillonite while zeolite and other phases were present in the 200 °C sample. Overall, more plutonium was desorbed from the 140 °C colloids (~9-16%), than from the 200 °C colloids (~4-8 %). Furthermore, at the end of the 4.5 day flow cell experiments, the desorption rates for the 140 °C colloids and the Pu-montmorillonite colloids were similar while the desorption rates from the 200 °C colloids were up to an order of magnitude lower. We posit that the formation of zeolites and clays hydrothermally altered at 200 °C may lead to a more stable association of plutonium with colloids, resulting in lower desorption rates. This may give rise to more extensive colloid-facilitated transport and help explain why trace levels of plutonium are found downgradient from their original source decades after a nuclear detonation. Interestingly, in the case of cesium (a co-contaminant of plutonium), no difference was observed between the 140 and 200 °C colloids. This reflects intrinsic differences between cesium and plutonium sorption/desorption behavior (charge, cation size), and suggests that the Cs sorption mechanism (cation exchange) is not similarly affected by colloid formation temperature.

LLNL-JRNL-764142

1. Introduction

Between 1951 and 1992, 828 underground nuclear tests were conducted at the Nevada National Security Site (NNSS), leaving behind a subsurface deposit of radionuclides consisting of tritium, fission products, activation products, and actinides.[1] Among the radionuclides deposited in the subsurface, plutonium (Pu) represents the most abundant anthropogenic element by mass (2.8 metric tons or 3.1×10^4 TBq).[1-3] In 1999, Kersting et al. [4] detected low levels of Pu in groundwater samples collected 1.3 km downgradient from an underground nuclear test at the NNSS and determined that the Pu is associated with the colloids, comprised primarily of clays and zeolite minerals. Additional groundwater samples from contaminated wells at the NNSS show a similar result with over 90% of the Pu associated with the inorganic colloids consisting of clays and zeolites[5]. Since that time, other studies have also shown Pu transport associated with both the inorganic and organic colloids.[6-11]

At the NNSS, the majority of the nuclear tests were conducted underground in silicic volcanic rocks of rhyolitic composition (75% SiO_2 and 15% Al_2O_3), with approximately 30% conducted below the water table.[1] The high temperatures and pressures achieved during an underground nuclear explosion vaporize and melt the surrounding rock.[12] During this process the overwhelming majority of the refractory radionuclides, including Pu, are incorporated into the melted rock[13, 14], also referred to as nuclear melt glass, which pools at the bottom of the test cavity.[12, 15] The initial groundwater temperatures and temperature histories in test cavities vary substantially. The Cambric nuclear test likely returned to ambient temperatures within a 10 years[16] while other tests, such as Almendro, recorded a downhole temperature of 157 °C, 23 years after detonation.[17] Plutonium, as well as other radionuclides (e.g. ^{137}Cs), will be released from the nuclear melt glass by dissolution during contact with groundwater.[18] Previous studies [19, 20] have shown that hydrothermal alteration of rhyolitic glasses of similar composition to those found at the NNSS leads to the formation of clay (e.g. smectite/montmorillonite) and zeolite (e.g. clinoptilolite-heulandite, analcime)[4, 21] secondary minerals, a fraction of which may be found in the form of colloids. Colloids, defined as particles ranging in size from 1 to 1000 nm, have low settling velocities and can remain suspended in solution for long periods of time. [22, 23] At the NNSS, the presence of fractured volcanic rock, high flow rates, and low ionic strength groundwater enhance colloid stability and potential migration.[4, 8, 24, 25] Although colloid facilitated transport has been recognized as the primary cause of Pu downgradient migration at this site,[4] the stability of Pu on these

LLNL-JRNL-764142

colloids has yet to be determined, limiting the conceptual understanding of the long-term migration potential of Pu at the NNSS.

To investigate the formation of colloids under NNSS conditions, Zavarin et al.[21] recently performed ~3-year hydrothermal alteration experiments on NNSS nuclear melt glass at four different temperatures (25, 80, 140 and 200 °C), and at ionic strength and pH conditions matching those typical of NNSS groundwater (0.7×10^{-3} mol/L $NaHCO_3$ and 5×10^{-3} mol/L NaCl and pH 8). After ~1000 days, both the 140 and 200 °C samples show significant glass alteration and colloid formation.[17] Elevated temperature increase glass alteration and colloid concentration and influence the mineralogy of the colloids. Montmorillonite (a smectite clay mineral) is the dominant crystalline phase formed at 140 °C; whereas, at 200 °C the colloidal fraction is composed of clays and zeolites (clinoptilolite, analcime). The concentration of Pu released from the altered melt glass also increases with temperature: Pu concentrations at 140 and 200 °C were up to three orders of magnitude higher than at room temperature and correlated with colloid concentration. The majority of Pu is associated with the colloidal fraction (~80%). The similar colloid mineralogy in these experiments and NNSS groundwater samples and the Pu association with these colloids, suggests that colloid-facilitated Pu transport is initiated by the hydrothermal alteration of Pu-containing nuclear melt glass.

The desorption rate of Pu plays a key role in determining the long-term transport of Pu on colloids [26-30]. Begg et al.[28] studied the desorption kinetics of Pu sorbed to SWy-1 montmorillonite using a flow cell (pH 4, 6, and 8 in a 0.7×10^{-3} mol/L $NaHCO_3$ and 5×10^{-3} mol/L NaCl buffer solution). Results show that the desorption of Pu is rate-limited but not irreversible. Based on batch sorption data and flow cell experiments[28, 31], Begg et al.[28] developed a numerical model to describe the sorption and surface mediated redox transformation of Pu(IV) and Pu(V) (Figure S1). Rate constants were determined for each sorption and desorption reaction and the model indicated an apparent Pu half-life on montmorillonite of 0.6–1.8 years. Results[28] show that Pu associated with clay colloids will migrate on the timescale of years to tens of years but not centuries, before Pu will completely desorb. However, the model [28] presumed that that nature of Pu associated with NNSS colloids is dominated by Pu adsorption to montmorillonite. Hydrothermal conditions in nuclear test cavities could lead to an alternative association of Pu with colloids (e.g. incorporation, irreversible association) that may increase the stability of Pu on colloids and increase the timescales of Pu migration from the NNSS.

In this study, we advance the work of Zavarin et al. [21] to explore the desorption rates of Pu and Cs from the 1000-days, hydrothermally produced nuclear melt glass colloids. Flow cell

LLNL-JRNL-764142

experiments were conducted with colloid suspensions produced from hydrothermal alteration of nuclear melt glass at pH 8. Three different suspensions were used for the flow cell experiments: (a) colloidal material from hydrothermal alteration of nuclear melt glass at 140 °C (140-Coll), (b) colloidal material from hydrothermal alteration of nuclear melt glass at 200 °C (200-Coll), and (c) ^{238}Pu sorbed to SWy-1 montmorillonite for ~8 months at room temperature (*SWy*). The objective of this work is to advance the understanding of 1) the underlying mechanism(s) controlling Pu behavior during hydrothermal alteration of nuclear melt glass, and 2) the fate of Pu colloid facilitated transport at environmentally relevant timescales (10s-100s years).

LLNL-JRNL-764142

2. Experimental

2.1 Materials and solutions

Preparation of the nuclear melt glass-derived colloids The original nuclear melt glass was retrieved from underground nuclear test debris samples available at Lawrence Livermore National Laboratory (LLNL). Details of the nuclear melt glass preparation and characterization can be found in Zavarin et al. (2019)[21] and in the SI. Melt glass samples were hydrothermally altered in passivated titanium pressure vessels (mod. 4764, Parr Instrument Company) for up to ~1000 days, at temperatures of 25, 80, 140 and 200 °C. After the hydrothermal alteration experiments, the colloidal material was washed three times with Milli-Q water (18.2 MΩ·cm) and stored as 15 mL suspensions in 50 mL centrifuge polypropylene tubes at room temperature for about 2.5 years.

Preparation of colloids for flow cell experiments Unless stated otherwise, all solutions were prepared with ultrapure Milli-Q water using ACS grade chemicals without further purification. For this study, colloidal material formed by hydrothermal alteration of melt glass at 140 and 200 °C in Zavarin et al. (2019)[21] was used. The original 15 mL suspensions were diluted to a total volume of 40 mL with Milli-Q water, shaken by hand and ultrasonicated (Branson 1800 ultrasonic cleaner) for 1 h to disaggregate the particles. After a ten-minute settling time, 30 mL of each suspension was transferred into 50 mL centrifuge tubes and centrifuged at 10,000 g for 8 h (Allegra® 21R, Beckman Coulter). After centrifugation, the supernatant was discarded, and the remaining solids (particles > 20 nm) were dried overnight in a heat block at 50 °C. The dried solids were resuspended in a background electrolyte to yield 1 g/L suspensions (0.7×10^{-3} mol/L $NaHCO_3$ and 5×10^{-3} mol/L NaCl at pH 8). The 1 g/L suspensions were left on a horizontal shaker (3527 Environ Orbital Incubator Shaker, Lab-Line Instruments) to equilibrate for at least one week until they were used in flow cell experiments (Table 1). Two flow cell experiments for each of the 140-Coll and 200-Coll suspensions were executed and will be referred to as *140**A***, *140**B***, *200**A*** and *200**B*** (Table 1). For comparison to the nuclear melt glass-derived colloids, a third system was studied using ^{238}Pu that had been previously sorbed for ~8 months to a montmorillonite colloid suspension of purified SWy-1 (referred to as *SWy*) and prepared as described in the SI. Aliquots of 140-Coll and 200-Coll and *SWy* were characterized by Scanning Electron Microscopy (SEM, FEI Inspect-F, operating voltages: 15kV), X-ray diffraction (XRD; Bruker D8- X-ray diffractometer, Cu Kα radiation), trace elements (quadrupole inductively coupled plasma mass spectrometry (ICP-MS)), zeta potential and dynamic light scattering (DLS)

LLNL-JRNL-764142

measurements. Details regarding the preparation and characterization of these colloidal materials are reported in the SI.

2.2 Desorption experiments

Similar to the studies of Tinnacher et al.[32] and Begg et al.[28], a flow cell was used to quantify Pu desorption from colloids as a function of time. The flow cell is made of polytetrafluoroethylene (PTFE) and consists of two parts: a 20 mL hemispherical lower chamber equipped with a small stir bar, and an upper part fitted on the lower chamber with an O-ring and screws. A PTFE filter (100 nm, Millipore) was installed to prevent colloids from exiting the flow cell. A high-performance liquid chromatography pump (mod. 307 Gilson, Inc.) was used to pass Pu-free background electrolyte through the flow cell and desorption rates were determined based on effluent Pu concentrations. Prior to each flow cell experiment, effluent sampling reservoirs (500-mL perfluoroalkoxy alkane jars; Savillex corporation) were cleaned with boiling 5% HNO_3 and boiling Milli-Q water, and flow cell components were rinsed with 10% HCl and Milli-Q water.

The following procedure was used for each flow cell experiment. Following a pre-equilibration period ($t_{\text{pre-equilibration}}$, Table 1), ~20 mL of a suspension was loaded into the flow cell and placed on a magnetic stirrer. The stir bar speed was kept low to minimize mineral grinding effects. Background electrolyte was pumped through the cell at a constant rate of 0.4 mL/min, which corresponded to an average retention time in the flow cell of 50 min. Effluent reservoirs were replaced twice per day and weighed. In total, 9 effluent samples were collected for each experiment. Each flow cell experiment was conducted for about 4.5 days. The pH and the redox potential, E_h (mV), of the influent and effluent were measured regularly. Speciation was calculated using PhreeqC[33] and the thermodynamic data compiled in ThermoChimie. [34, 35]

After pre-equilibration and prior to loading the suspension into the flow cell, the colloidal suspension was sampled to determine the initial total and aqueous Pu concentration (Table S1). To determine the aqueous Pu concentration, an aliquot of the suspension was centrifuged at 10,000 *g* for 2 h to remove particles > 20 nm, and the supernatant was analyzed (Section 2.3). Following the completion of each experiment, the suspension was removed from the flow cell and transferred to a 50-mL centrifuge tube. The tube was placed on a horizontal shaker at 125 rpm in the dark at room temperature for a period of > 6 months ($t_{\text{long-term}}$, Table 2). The total and aqueous Pu concentrations in each of the suspensions were then re-measured.

LLNL-JRNL-764142

For selected flow cell experiments (*140A*, *140B*, and *200A*), the first effluent sample was checked for the presence of colloids. Approximately 50 % of the effluent solution was transferred into 250-mL centrifuge tubes (PP; Corning Inc.) and centrifuged (Allegra® 6KR, Beckman Coulter) at 3210 *g* for 25 h to remove particles in the 20-100 nm range. The Pu concentration in the supernatant was measured and compared to the bulk Pu concentration.

2.3 Determination of $^{239+240}$Pu and ^{238}Pu

All $^{239+240}$Pu concentrations in *140A*, *140B*, *200A* and *200B* experiments were measured using multi-collector inductively coupled plasma mass spectrometry (MC ICP–MS; mod. Nu Plasma, CAMECA Instruments, Inc.). The detailed methodology for the sample preparation is reported in the SI. All ^{238}Pu concentrations in the *SWy* experiment were determined using liquid scintillation counting (LSC; Tri-Carb 2900TR liquid scintillation analyzer, PerkinElmer). Every other effluent sample from each experiment was analyzed for $^{239+240}$Pu or ^{238}Pu (see Section 2.4). In addition, the total and aqueous $^{239+240}$Pu or ^{238}Pu concentrations prior to the start of the experiments (i.e. initial samples) and after the completion of the experiments (i.e. long-term samples) were measured. Procedural blanks were routinely processed and analyzed.

2.4 Determination of ^{137}Cs

Cesium (^{137}Cs) desorption was also quantified in the *140A*, *140B*, *200A* and *200B* experiments. The initial suspension, as well as every sample that was not processed for Pu analysis (see Section 2.3), were analyzed for their ^{137}Cs content (5 samples per run) via γ-spectroscopy (broad energy high-purity germanium detector, Canberra Industries, Inc.). All spectra were analyzed with the software Genie 2000 (Canberra). Energy and efficiency calibrations were conducted on the γ-peak of ^{137}Cs at 661.657 keV.

2.5 Simulation of desorption kinetics

The model described in detail in Begg et al. (2017)[28] was used to simulate the desorption of Pu. In this model, the aqueous Pu ($Pu(V)_{aq}$ and $Pu(IV)_{aq}$) and sorbed Pu ($Pu(V)_{S1}$ and $Pu(IV)_{S2}$) was considered along with the kinetics of sorption and surface-mediated redox transformations (Figure S1).[31] A second Pu(IV) sorbed species, $Pu(IV)_{S3}$, was considered in the model to account for aging processes other than redox reactions.[28] Model equations, model input parameters, and a schematic overview of the reactions included in the model are described in detail in the SI.

In their original fitting of Pu desorption from SWy-1 montmorillonite, Begg et al.[28] linked

their flow cell code to the PEST (Parameter ESTimation) code.[36] Using PEST, optimized model parameters using least square minimization based on the Gauss-Marquardt-Levenberg method were determined. At pH 8, four sets of fitted parameters were reported (*3weeks*, *3weeks-ψ*, *6months*, *6months-ψ* Table S2). Importantly, each of these four PEST optimizations includes a covariance matrix for the fitted parameters (Table S3).

In the present study Pu desorption was simulated using the four sets of fitted model parameters from Begg et al.[28], and the parameters were fixed at all times (Table S1) . The simulations were run in two steps. In the first step, Pu distribution on $Pu(V)_{S1}$, $Pu(IV)_{S2}$ and $Pu(IV)_{S3}$ was determined considering the 2.5 year storage of the original suspension prior to the start of the flow-cell experiment (Table 1, Table S4). In the second step, the Pu distribution on the three sorption sites was used as a starting condition to simulate the pre-equilibration ($t_{\text{pre-equilibration}}$, Table 1), desorption of Pu during the flow cell experiment (~4.5 days), and the long-term equilibration at the end of the experiment ($t_{\text{long-term}}$, Table 2).

For each of the four parameter sets reported in Begg et al.[28] (*3weeks*, *3weeks-ψ*, *6months*, *6months-ψ*) and each of the 5 desorption experiments described here, PEST was used to generate 100 realizations of Pu desorption based on the parameters, parameter uncertainties, and associated parameter covariance matrix (Table S3). This was accomplished by using the PEST RANDPAR functionality which generates parameter realizations based on the parameters, parameter uncertainties and associated parameter covariance matrix. Simulation results presented and discussed in this work represent the average of these 100 realizations for each of the four sets of fitted parameters reported in Begg et al.[28] Model errors represent the 95th percentile of the values calculated at each sampling point.

A linear uncorrelated uncertainty test was performed for experiment *140A* only. Here, the PEST RANDPAR functionality was used to generate 100 realizations without accounting for parameter covariance. This test was performed to evaluate the importance of parameter covariance on estimated model uncertainties. Results showed that inclusion of the covariance matrix from the original model[28] significantly reduced the apparent model uncertainty (Figure S2). This is an indication that fitted parameters were strongly correlated and that model uncertainty is not adequately captured without the accounting of parameter covariance.

LLNL-JRNL-764142

3. Results and Discussion

3.1 Characterization of mineral colloids

The *SWy*, 140-Coll, and 200-Coll colloids were characterized by XRD (SI). The XRD pattern of *SWy* matched the montmorillonite reference pattern from the International Center for Diffraction Data (data not shown). Oriented P-XRD samples were prepared in air-dried and ethylene glycol saturated form to determine the nature of the 140-Coll and 200-Coll colloids.[37] The results suggest that both samples probably contain mixed layer clays, most likely an illite/smectite(montmorillonite)[37] (Figure S3, 4 and 5). There is a shift towards higher degrees of 2θ of the diffraction peaks in the 200-Coll air-dried and solvated sample which may be indicative of higher degree of illitization.[37] Hydrothermal conditions during diagenesis have been shown to cause montmorillonite recrystallization to non-expandable clays, or clays with mixtures of expandable and non-expandable layers (i.e. beidellite, illite).[38-40] In the 200-Coll sample, the zeolite heulandite was identified, together with additional unassigned peaks between 13-16° of 2θ (Figure S4). SEM images of 200-Coll revealed the presence of euhedral tabular crystals (Figure S6) with a clay-like composition (energy-dispersive semi-quantitative analysis: Si 33.0±2.5%, Al 9.9±1.0%). Formation of zeolite is expected to occur during alteration of Si-rich glasses under hydrothermal temperature regimes.[19, 41] Overall, the mineralogy of 140-Coll and 200-Coll is consistent with mineralogical characterization of the altered volcanic rocks and colloids present in NNSS groundwaters.[4, 42] 140-Coll, 200-Coll and *SWy* contain elevated Fe content Fe (1.2-3% wt., Table S5). SEM images reveal that most of the colloids are in 100-1000 nm size range [21], which is consistent with DLS characterization (Figure S7, Table S6). Further details can be found in SI.

3.2 Characterization of initial suspensions

The pH as well as the total and aqueous Pu concentrations were measured before the start of each flow cell experiment (Table 1 and S1). The log $K_{\mathrm{d\ initial}}$ (m^3/kg) values for each experiment were calculated (Table 1). In *SWy*, the log $K_{d\ \mathrm{initial}}$ (m^3/kg) was 1.32±0.05 (Table 1). Begg et al.[28] reported K_d values for Pu(IV) sorbed to montmorillonite equilibrated for 3 weeks (log K_d (m^3/kg) = 0.94) and 6 months (log K_d (m^3/kg)= 1.46). Here, *SWy* was equilibrated for 248 days (~8 months, Table 2), and the log K_d is in good agreement with the 6 month K_d reported by Begg et al.[28] The log $K_{d\ \mathrm{initial}}$ values in ***140A*** and ***140B*** (2.02±0.16 and 1.83±0.12, respectively) are somewhat higher than in ***200A*** and ***200B*** (1.70±0.15

LLNL-JRNL-764142

1.70±0.08, respectively) and overall higher than the K_d values for *SWy*. However, these values are broadly in agreement with K_d values reported for FEBEX bentonite (log K_d (m^3/kg) = 1.3-1.9)[29] and montmorillonite (log K_d (m^3/kg) = 0.94-1.46) [28, 29, 31]. Figure S8 shows the surface charge of 140-Coll, 200-Coll and *SWy* measured as a function of pH. All three samples exhibit an increasingly negative charge with increasing pH. The surface charge of 140-Coll and *SWy* at pH ~ 8 is identical within error (-39±1 mV), however 200-Coll has a significantly lower surface charge (-54 mV). The difference in surface charge may be related to the differences in mineralogy between the samples, as zeolites and an unidentified clay are present in the 200-Coll, but absent in 140-Coll. [43, 44] These results suggest that hydrothermally formed clay colloids, particularly those produced at higher temperatures, may not behave identically to SWy-1.

3.3 Flow-cell desorption experiments

The effluent ^{239,240}Pu and ^{137}Cs concentrations in the *140**A***, *140**B***, *200**A*** and *200**B*** experiments, and the effluent ^{238}Pu concentration in the *SWy* experiment are plotted in Figure 1. After 4.5 days, 10.7±0.3% of ^{238}Pu was desorbed in the *SWy* experiment (Figure 1 and Table 2). The Pu desorption behavior observed in *140**A*** and *140**B*** follow *SWy* very closely (Figure 1); in these experiments, 15.5±0.3% and 8.8±1% Pu was desorbed, respectively (Table 2). In *200**A*** and *200**B***, 4.1±0.5% and 7.8±1.0% of Pu desorbed, respectively. While the total percentage of Pu desorbed during these flow cell experiments is only somewhat lower in the *200**A/B*** experiments (total percent desorbed is controlled in large part by the Pu concentrations measured at the start of each flow cell experiment), the difference in effluent Pu concentration in the *140**A/B*** and *200**A/B*** experiments is clearly discernible at the end of each experiment (Figure 1) and indicative of differences in the underlying desorption mechanisms. In fact, the effluent Pu concentrations in *200**A**/**B*** were up two orders of magnitude lower than in *140**A**/**B***, and *SWy* (Figure 1) at the end of their respective experiments.

Differences between *140**A*** and *140**B*** and differences between *200**A*** and *200**B*** (Figure 1) may be related to differences in $t_{\text{pre-equilibration}}$ (i.e. aging effects), small variations in S/L ratio, or inherited mineralogical inhomogeneities of colloidal materials sampled. It is expected that aging effects may result in lower Pu desorption. This is consistent with observations from the *140**A**/**B*** experiments where less Pu is desorbed from *140**B*** (288 days equilibration, 8.8%), compared to a *140**A*** (5 days equilibration, 15.5%) (Table 1 and 2). Comparing experiments

LLNL-JRNL-764142

that equilibrated for similar times (both *140A* and *200A* were equilibrated for 5 and 7 days respectively) only 4.2% Pu is desorbed in *200A* compared to 15% in *140A*. Considering that both experiments were conducted with similar flow rate, solid: solution ratio and for similar amounts of time (or ~130 pore volumes) this difference in Pu desorption is most likely indicative of a different mechanism controlling Pu desorption in the two suspensions. Details on how the % of Pu desorbed were calculated can be found in the SI.

For three experiments (*140A*, *140B* and *200A*), the first effluent sample was tested to determine the presence of 20-100 nm colloidal particles. 11-12% of the total Pu was associated with 20-100 nm colloids in the *140A*/*B* experiments. In *200A*, ~8% of the total Pu associated was associated with 20-100 nm colloids. These results confirm that ~90% of Pu in the flow cell effluent is present as aqueous. For the purposes of this work, we consider the Pu measured in flow cell effluent as dissolved.

3.4 Characteristics of long-term suspensions

After a time period > 6 months ($T_{long\text{-}term}$, Table 2), the suspension from each flow cell was re-analyzed for its Pu content (total and aqueous). The aqueous Pu concentration in all suspensions was found to have increased compared to the Pu concentration measured in the last fraction of the flow-cell experiments (4.5 days) (Table S1). An increase in the long-term Pu aqueous concentrations is consistent with experimental data reported in Begg et al.[28] and indicative of slow desorption. Based on these results, the log $K_{d\ \text{long-term}}$ (m^3/kg) values were calculated (Table 2) and were found to be 2.45±0.03, 2.38±0.03 and 2.22±0.04 for *140A*, *140B* and *SWy,* respectively. These $K_{d\ \text{long-term}}$ values are 2-4 times greater than the $K_{d\ \text{initial}}$ for the same sample (Tables 1 and 2). The log $K_{d\ \text{long-term}}$ (m^3/kg) for *200A* and *200B* are 2.88±0.03 and 3.78±0.04, respectively which reflect an increase in $K_{d\ \text{long-term}}$ up to one order of magnitude from the $K_{d\ \text{initial}}$ (Tables 1 and 2). Given the loss of Pu during the flow cell experiment and the S/L ratio uncertainties associated with the transfer of suspensions from the flow cell container to allow solution aging, it is not possible to make quantitative comparison between the initial and long-term K_d that would allow a determination of whether Pu desorption was truly non-reversible under these conditions. Nonetheless these measurements provide some insights into the different Pu desorption kinetics from these colloids indicating a slower desorption of Pu from the colloids formed at 200 °C.

3.5 Desorption of Cs

The initial total ^{137}Cs concentration amounted to $(1.72\pm0.14)\times10^{-12}$ mol/L for *140A* and

LLNL-JRNL-764142

(2.16±0.17)×10^{-12} mol/L for the *200A* colloidal suspensions. As shown in Figure 1b there are no significant differences in the effluent ^{137}Cs concentrations in the *140A/B* and *200A/B* experiments. In total, ~44% (*140A*) and ~37% (*200A*) of ^{137}Cs desorbed by the end of the experiment. For *140A* and *140B*, the ratio of desorbed ^{137}Cs/^{239,240}Pu amounted to ~0.05 and ~0.01, respectively. In contrast to the *140A/B* experiments, the ^{137}Cs/^{239,240}Pu ratio in the *200A/B* experiments is significantly higher (0.57 for *200A*; 1.75 for *200B*) reflecting the experimental observation that much less Pu desorbed from 200-Coll (Figure 1a).

3.6 Desorption mechanisms

Cesium sorption onto clay and zeolites is likely controlled by cation exchange mechanisms.[45, 46] Temperature of colloids formation has an impact on the surface charge of the material (Figure S8), however the temperature of colloid formation does not appear to have an effect on the desorption of Cs from nuclear melt glass-derived colloids (Figure 1b). This suggests that Cs sorption/desorption processes in hydrothermally altered colloids are controlled by a similar reversible mechanism, most likely involving cation exchange processes.

In contrast, the effluent Pu concentrations in the *200A/B* experiments are up to two orders of magnitude lower than the Pu concentrations in the *SWy* and *140A/B* experiments (Figure 1). This difference in desorption behavior suggests that the mechanism of Pu interaction with 200-Coll may differ from 140-Coll and *SWy.* Differences in desorption behavior may be related to differences in Pu speciation, variations in mineralogy and materials properties, or a mechanism besides sorption to montmorillonite, as described below.

The oxidation state of Pu, present as Pu(IV) or Pu(V), will impact the affinity of Pu for mineral surfaces. [31, 47-49] The 140-Coll and 200-Coll were produced from hydrothermal alteration of the same nuclear melt glass, in similar geochemical conditions and are characterized by similar Pu total and aqueous concentrations (Table S1). Although the Pu oxidation state in solution was too low to be determined experimentally, speciation calculations indicate that Pu in 140-Coll, 200-Coll and *SWy* solutions is similar and dominated by $Pu(OH)_4$ and PuO_2^+ species. This suggests that any potential differences in Pu speciation would be small and not responsible for the desorption variations observed experimentally (Table S8).

In contrast to 140-Coll, 200-Coll is characterized by different surface properties (Figure S8) and complex mineralogy. In 200-Coll, Pu will not only interact with montmorillonite but also the zeolites, and tabular clay minerals (Figure S6). The K_d for Pu sorption to montmorillonite is typically higher than for zeolite.[50] Nevertheless, the average long-term K_d (Table 2)

LLNL-JRNL-764142

determined at the end of the ***200A/B*** experiments (3.3 m^3/kg) is substantially higher than in the ***140A/B*** (2.4 m^3/kg) and the *SWy* (2.2 m^3/kg) experiments and the desorption kinetics follow a similar pattern (i.e. slower kinetics in ***200A/B*** experiments). Hydrothermal alteration of nuclear melt glass at 200 °C results in the formation of a material with a highly negative surface charge and mixed mineralogy (zeolite and various clay minerals). It can be speculated that this material strongly retains Pu either as "aged" sorbed species (i.e. higher Pu content on $Pu(IV)_{s3}$ and/or Pu sequestrated in the zeolite structure or the clay interlayers (illite/smectite and tabular clay minerals (Figure S6)). This stronger association likely leads to lower Pu desorption kinetics on the 200-Coll colloids.

3.7 Modeling results

In order to test the validity of the Begg et al.[28] model for our colloidal suspensions, the Pu desorption behavior for all five flow cell experiments was simulated. For *SWy*, the model parameters that best capture Pu desorption behavior were from the *3weeks-ψ* model (Figure 2). The other models (*3weeks*, *6months*, *6months-ψ*) captured the overall desorption behavior but Pu concentrations at each time point were slightly underestimated (Figure S9). The *3weeks-ψ* model was also the best fit model for the data reported by Begg et al.[28] For these reasons, the *3 weeks-ψ* model was used here to simulate and compare the Pu desorption behavior for experiments *140**A***, *140**B***, *200**A***, and *200**B***. Simulations using the other three models are reported in Figure S10.

Overall, the ***140A/B*** experiments showed similar Pu desorption behavior as the *SWy*, in particular ***140A*** (Figure 1). The simulated desorption behavior for ***140A*** and ***140B*** are presented in Figure 3a and b, respectively. Broadly, the simulated desorption behavior in the ***140A/B*** experiments follow the trends of *SWy* with a good, though slightly underestimated, prediction of Pu desorption at the end of the flow cell experiment. While there are significant differences in desorption behavior in the ***200A*** and ***200B*** experiments, model simulations drastically overestimate the rates of Pu desorption (Figure 3c and d). The simulations indicate that the model[28] effectively captures Pu desorption from the *SWy* and ***140A/B***. However, the mismatch between simulated and observed desorption rates in the ***200A/B*** experiments suggest the presence of sorption mechanisms that are missing in the Begg et al. model. Based on our detailed examination of the modeling results, the initial desorption of Pu (0-2 days) is mainly controlled by the desorption of Pu(V) ($Pu(V)_{S1} \rightarrow Pu(V)_{aq}$). In this timeframe, the model matches the data for all experiments quite well. Poorer model fits are observed after day 2, especially for 200-Coll. After day 2, the rate (and slope) of the simulated Pu

LLNL-JRNL-764142

desorption is controlled by the rate of Pu(IV) desorption ($Pu(IV)_{S2} \rightarrow Pu(IV)_{aq}$) and kinetics between $Pu(IV)_{S3}$ and $Pu(IV)_{S2}$ ($Pu(IV)_{S3} \rightarrow Pu(IV)_{S2}$), where $Pu(IV)_{S3}$ represents the most stable fraction of Pu on the mineral surface. It would, therefore, appear that reaction kinetics of these more stable components of sorbed Pu account for the major differences in the simulated and measured Pu desorption behavior in all cases.

The simulated log $K_{d\ \mathrm{initial}}$ (m^3/kg) and log $K_{d\ \mathrm{long\text{-}term}}$($m^3$/kg) are calculated using the geometric mean of the output 100 model simulations and are statistically identical (Table 2). The simulated log $K_{d\ \mathrm{initial}}$ is in reasonable agreement with experimental log $K_{d\ \mathrm{initial}}$ for all experiments (*140**B*** is within the errors while others are slightly overestimated). Differences in desorption behavior can be identified in the log $K_{d\ \mathrm{long\text{-}term}}$ values. The simulated log $K_{d\ \mathrm{long\text{-}term}}$ for *SWy* is consistent with experimental data. The simulated log $K_{d\ \mathrm{long\text{-}term}}$ for *140**A**/**B*** are slightly lower than the measured values. However, the simulated log $K_{d\ \mathrm{long\text{-}term}}$ for *200**A**/**B*** are up to one order of magnitude lower than the measured values. These modeling results confirm that Pu desorption from the 200-Coll colloids is overestimated using the model[28], suggesting that simple montmorillonite sorption/desorption does not fully capture Pu desorption behavior of colloids formed at 200 ºC.

3.8 Environmental implications

The results of this study suggest that Pu desorption rates from nuclear melt glass colloids are affected by the hydrothermal conditions during colloid formation. The desorption rates of Pu from the colloids formed at 140 °C can be effectively predicted based on montmorillonite thermodynamic and kinetic sorption/desorption at ambient temperatures. The formation of zeolites and clays at the higher temperature may lead to more stable Pu associations with colloids, resulting in the lower desorption rates. The temperature history of individual underground nuclear tests at the NNSS can vary substantially. If hydrothermal conditions are short-lived, the desorption of Pu from colloids may be effectively predicted based on Pu desorption from montmorillonite.[28] However, if temperatures remain elevated for years (≥ 200 °C), hydrothermal alteration of the nuclear melt glass may lead to formation of additional colloidal phases (zeolites and tabular clay minerals (Figure S6)). Pu associated with these additional phases may give rise to the lower desorption rates. Although both mechanisms may be operating at the NNSS, the Pu association with montmorillonite colloids would limit colloid-facilitated transport of Pu on the order of years to possibly a few decades. Begg et al.[28] estimated the "half-life" of Pu on colloids, based on montmorillonite desorption kinetics, to be in the order of 0.6-1.8 years. As the desorption kinetic of Pu in 200-Coll are

LLNL-JRNL-764142

underestimated by the model by at least one order of magnitude, the "half-life" of Pu on this material is likely to be on the orders of decades, rather than years. The results of this work highlight multiple ways in which Pu may migrate in the environment and may help explain why trace levels of Pu are found in certain downgradient wells at the NNSS many decades after the termination of underground nuclear testing (September 23, 1992).

Table 1: Initial conditions of the nuclear melt glass colloidal suspensions.

Colloidal suspension	$t_{pre\text{-}equilibration}$[a] (days)	$S/L_{initial}$ (g/L)[b]	$pH_{initial}$[c]	log $K_{d\ initial}$ (m^3/kg)[d]	Pu in aqueous phase (%)[e]
140A	5	1.025	7.91	2.02±0.16	1.4±0.2
140B	288	1.025	8.01	1.83±0.09	0.9±0.2
200A	7	1.066	8.11	1.70±0.05	1.8±0.3
200B	74	1.066	7.86	1.70±0.17	1.8±0.3
SWy	248	0.978	7.92	1.32±0.05	4.6±0.3

[a] Time of pre-equilibration of the colloidal suspensions in background electrolyte solution before the start of the flow cell experiment.

[b] Solid-to-liquid ratio of the suspension before loading in the flow cell.

[c] pH of the colloidal suspensions before the start of the flow cell experiment.

[d] initial distribution coefficient for Pu measured after $t_{pre\text{-}equilibration}$ and prior to filling the suspension in the flow cell. The $S/L_{initial}$ was used to calculate these values (2σ represents the propagation of analytical uncertainties).

[e] Pu in aqueous phase (%) measured after $t_{pre\text{-}equilibration}$ and prior to filling the suspension in the flow cell. (2σ represents the propagation of analytical uncertainties).

Table 2: Solution conditions during and after flow cell experiments.

Colloidal suspension	$S/L_{flow\ cell}$[a] (g/L)	$t_{long\text{-}term}$[b] (days)	% Pu desorbed (4.5 days)[c]	log $K_{d\ long\text{-}term}$ (m^3/kg)[d]	Simulated log $K_{d\ initial}$ (m^3/kg)[e]	Simulated log $K_{d\ long\text{-}term}$ (m^3/kg)[f]
140A	0.794	242	15.5±0.3	2.45±0.03	2.16±0.10	1.91±0.17
140B	0.814	191	7.1±1.0	2.38±0.03	2.05±0.15	2.15±0.16
200A	0.867	498	4.2±0.5	2.88±0.03	2.13±0.11	2.07±0.15
200B	0.836	431	7.8±1.0	3.78±0.04	2.12±0.09	2.08±0.15
SWy	0.750	274	10.7±0.3	2.22±0.04	2.05±0.15	2.08±0.15

[a] Solid-to-liquid ratio inside the flow cell due to dilution with the influent.

[b] Time of suspension equilibration after the flow cell experiment.

[c] % of Pu in solution after 4.5 days of desorption (2σ represents the propagation of analytical uncertainties).

[d] Pu distribution coefficient at $t_{long\text{-}term}$. (2σ represents the propagation of analytical uncertainties).

[e] Simulated initial distribution coefficient for Pu (*3 weeks-ψ)*. (2σ of the averaged geometric mean of 100 simulated model outputs)

[f] Simulated long-term distribution coefficient for Pu (*3weeks-ψ*). (2σ of the averaged geometric mean of 100 simulated model outputs)

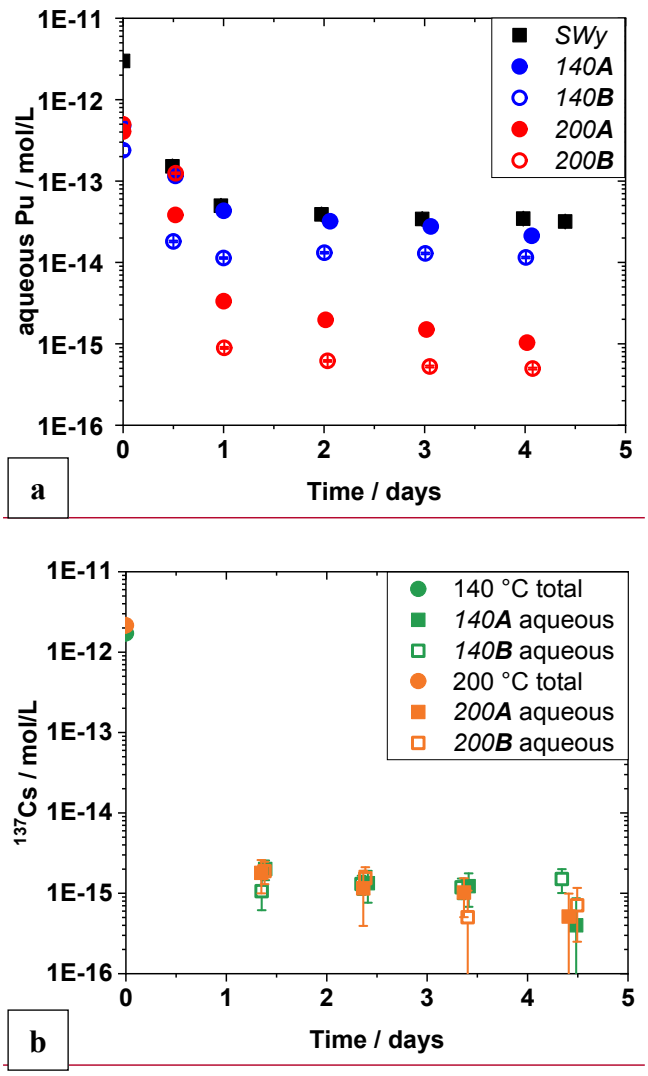

Figure 1: Concentration of Pu and Cs detected in the effluent reservoirs of the flow cell as a function of time: (a) Pu desorbed from *SWy*; *140**A,B***; *200**A,B***; (b) ^{137}Cs desorbed from *140**A,B***; *200**A,B***. (errors: 2σ).

LLNL-JRNL-764142

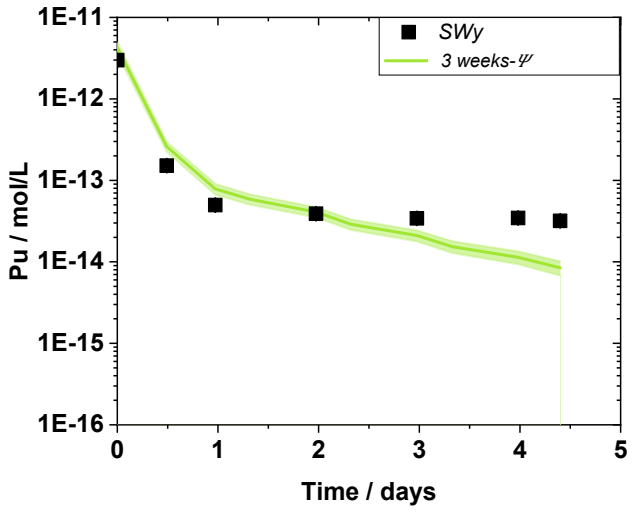

Figure 2: Modelling results of *3weeks-ψ* compared to *SWy* experimental data (black squares). Light green area represents the model confidence (2σ).

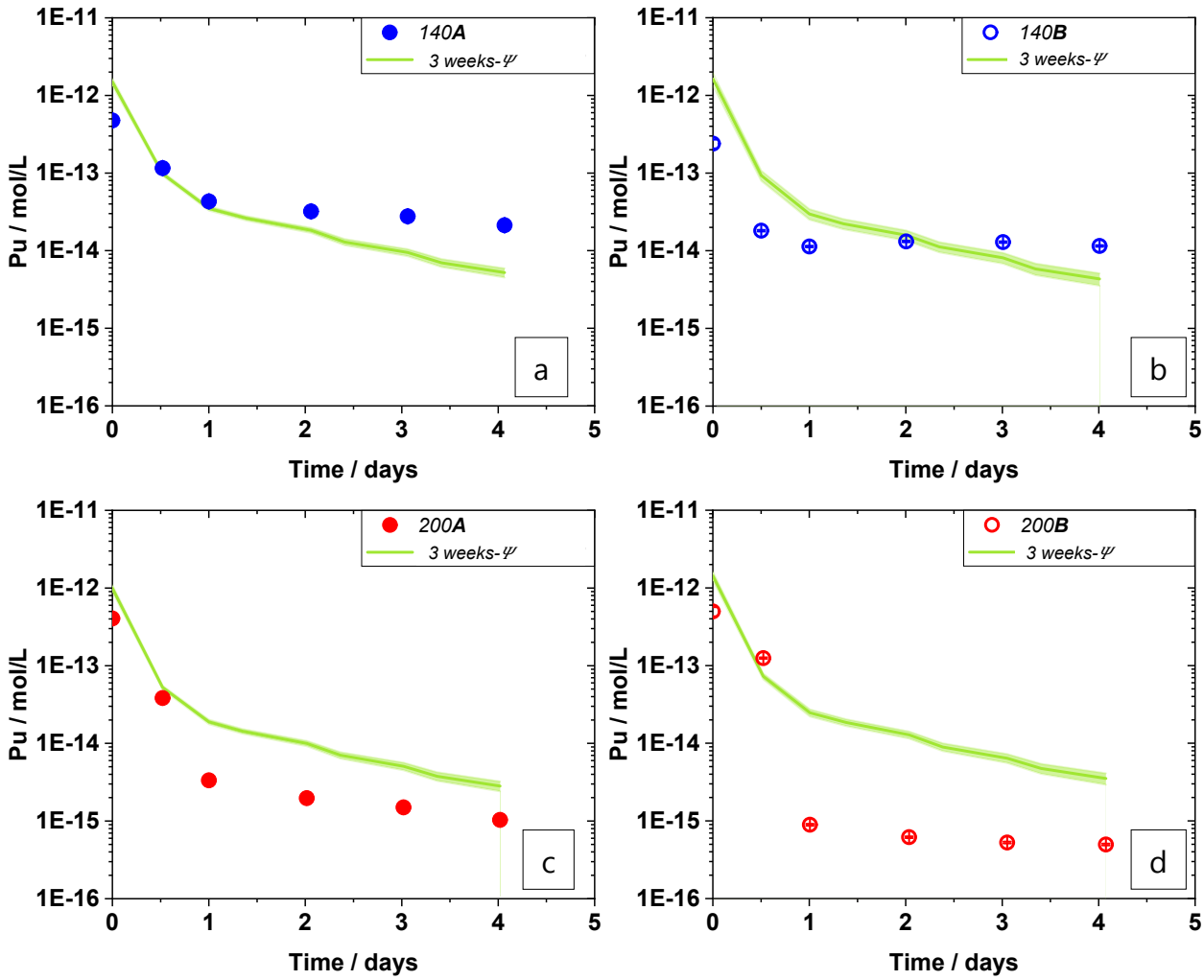

Figure 3: Modelling results of *3weeks-ψ* (lines) compared to *140A* (a), *140B* (b), *200A* (c), and *200B* (d). Light green area represents the model confidence (2σ).

LLNL-JRNL-764142

Acknowledgements

This work was supported by the Subsurface Biogeochemical Research Program of the U.S. Department of Energy's Office of Biological and Environmental Research. The manuscript was prepared under the auspices of the U.S. Department of Energy by Lawrence Livermore National Security, LLC under contract DE-AC52-07NA27344. We thank B. Powell (Clemson University, SC) for providing the flow cells, J. Begg for helpful advice on running the flow cell, C. Durrant for purification of the SWy-1 montmorillonite, T. Parsons-Davis and T. Woody for help with γ-spectroscopy, K. Morrison for help in preparing clays for P-XRD measurements, V. Montoya for advice in thermodynamic databases, and R. Williams for support with the MC ICP–MS measurements. LLNL-JRNL-764142.

References

1. Smith, D. K.; Finnegan, D. L.; Bowen, S. M., An inventory of long-lived radionuclides residual from underground nuclear testing at the Nevada test site, 1951-1992. *Journal of Environmental Radioactivity* **2003,** *67*, (1), 35-51.
2. Smith, D. K.; Williams, R. W., The dynamic movement of plutonium in an underground nuclear test with implications for the contamination of groundwater. *Journal of Radioanalytical and Nuclear Chemistry* **2005,** *263*, (2), 281-285.
3. Bowen, S. M.; Finnegan, D. L.; Thompson, J. L.; Miller, C., M.; Baca, L. F.; Geoffrion, C. G.; Smith, D. K.; Goishi, W.; Esser, B. K.; Meadows, J. W.; Namboodiri, N.; Wild, J. F. *Nevada Test Site radionuclide inventory, 1951-1992*; Los Alamos National Laboratory: Los Alamos, NM, 2001.
4. Kersting, A. B.; Efurd, D. W.; Finnegan, D. L.; Rokop, D. J.; Smith, D. K.; Thompson, J. L., Migration of plutonium in ground water at the Nevada Test Site. *Nature* **1999,** *397*, (6714), 56-59.
5. Zhao, P. H.; Zavarin, M.; Leif, R. N.; Powell, B. A.; Singleton, M. J.; Lindvall, R. E.; Kersting, A. B., Mobilization of actinides by dissolved organic compounds at the Nevada Test Site. *Applied Geochemistry* **2011,** *26*, (3), 308-318.
6. Santschi, P. H.; Roberts, K. A.; Guo, L. D., Organic nature of colloidal actinides transported in surface water environments. *Environmental Science & Technology* **2002,** *36*, (17), 3711-3719.
7. Novikov, A. P.; Kalmykov, S. N.; Utsunomiya, S.; Ewing, R. C.; Horreard, F.; Merkulov, A.; Clark, S. B.; Tkachev, V. V.; Myasoedov, B. F., Colloid transport of plutonium in the far-field of the Mayak Production Association, Russia. *Science* **2006,** *314*, (5799), 638-641.
8. Wolfsberg, A.; Dai, Z. X.; Zhu, L.; Reimus, P.; Xiao, T.; Ware, D., Colloid-Facilitated Plutonium Transport in Fractured Tuffaceous Rock. *Environmental Science & Technology* **2017,** *51*, (10), 5582-5590.

9. Ikeda-Ohno, A.; Harrison, J. J.; Thiruvoth, S.; Wilsher, K.; Wong, H. K. Y.; Johansen, M. P.; Waite, T. D.; Payne, T. E., Solution Speciation of Plutonium and Americium at an Australian Legacy Radioactive Waste Disposal Site. *Environmental Science & Technology* **2014,** *48*, (17), 10045-10053.

10. Xu, C.; Athon, M.; Ho, Y. F.; Chang, H. S.; Zhang, S. J.; Kaplan, D. I.; Schwehr, K. A.; DiDonato, N.; Hatcher, P. G.; Santschi, P. H., Plutonium Immobilization and Remobilization by Soil Mineral and Organic Matter in the Far-Field of the Savannah River Site, US. *Environmental Science & Technology* **2014,** *48*, (6), 3186-3195.

11. Loyland Asbury, S. M.; Lamont, S. P.; Clark, S. B., Plutonium Partitioning to Colloidal and Particulate Matter in an Acidic, Sandy Sediment: Implications for Remediation Alternatives and Plutonium Migration. *Environmental Science & Technology* **2001,** *35*, (11), 2295-2300.

12. Smith, D. K., Characterization of Nuclear Explosive Melt Debris. *Radiochimica Acta* **1995,** *69*, (3), 157-167.

13. Eppich, G. R.; Knight, K. B.; Jacomb-Hood, T. W.; Spriggs, G. D.; Hutcheon, I. D., Constraints on fallout melt glass formation from a near-surface nuclear test. *Journal of Radioanalytical and Nuclear Chemistry* **2014,** *302*, (1), 593-609.

14. Holliday, K. S.; Dierken, J. M.; Monroe, M. L.; Fitzgerald, M. A.; Marks, N. E.; Gostic, R. C.; Knight, K. B.; Czerwinski, K. R.; Hutcheon, I. D.; McClory, J. W., Plutonium segregation in glassy aerodynamic fallout from a nuclear weapon test. *Dalton Transactions* **2017,** *46*, (6), 1770-1778.

15. IAEA *The Radiological Situation at the Atolls of Mururoa and Fangataufa: Main Report*; International Atomic Energy Agency: Vienna, 1998.

16. Carle, S. F.; Maxwell, R. M.; Pawloski, G. A.; Shumaker, D. E.; Tompson, A. B.; Zavarin, M. *Evaluation of the Transient Hydrologic Source Term for the Cambric Underground Nuclear Test at Frenchman Flat, Nevada test Site*; UCRL-TR-226916; TRN: US200721%%553 United States 10.2172/907859 TRN: US200721%%553 LLNL English; ; Lawrence Livermore National Lab. (LLNL), Livermore, CA (United States): 2006; pp Medium: ED; Size: PDF-file: 382 pages; size: 25.4 Mbytes.

17. Kersting, A. B.; Zavarin, M., Colloid Facilitated Transport of Plutonium at the Nevada Test Site, NV, USA. In *Actinide Nanoparticles Research*, Kalmykov, S.; Denecke, M. A., Eds. Springer-Verlag: 2011; pp 399-412.

18. Declercq, J.; Diedrich, T.; Perrot, M.; Gislason, S. R.; Oelkers, E. H., Experimental determination of rhyolitic glass dissolution rates at 40-200 degrees C and 2 < pH < 10.1. *Geochimica Et Cosmochimica Acta* **2013,** *100*, 251-263.

19. Gottardi, G., THE GENESIS OF ZEOLITES. *European Journal of Mineralogy* **1989,** *1*, (4), 479-487.

20. Hodder, A. P. W.; Naish, T. R.; Nelson, C. S., A 2-STAGE MODEL FOR THE FORMATION OF SMECTITE FROM DETRITAL VOLCANIC GLASS UNDER SHALLOW-MARINE CONDITIONS. *Marine Geology* **1993,** *109*, (3-4), 279-285.

LLNL-JRNL-764142

21. Zavarin, M.; Zhao, P.; Joseph, C.; Begg, J. D.; Boggs, M. A.; Dai, Z.; Kersting, A. B., Hydrothermal Alteration of Nuclear Melt Glass, Colloid Formation, and Plutonium Mobilization at the Nevada National Security Site, U.S.A. *Environmental Science & Technology* **2019**.

22. Stumm, W., *Chemistry of the solid-water interface: processes at the mineral-water and particle-water interface in natural systems*. New York, 1992.

23. Ryan, J. N.; Elimelech, M., Colloid mobilization and transport in groundwater. *Colloids and Surfaces A: Physicochemical and Engineering Aspects* **1996,** *107*, 1-56.

24. Blankennagel, R. K.; Weir, J. E., Jr. *Geohydrology of the eastern part of Pahute Mesa, Nevada Test Site, Nye County, Nevada*; U.S. Atomic Energy Commission: Washington, 1973.

25. Laczniak, R. J.; Cole, J. C.; Sawyer, D. A.; Trudeau, D. A. *Summary of hydrogeologic controls on ground-water flow at the Nevada Test Site, Nye County, Nevada*; U.S. Geological Survey: Carson City, Nevada, 1996.

26. Tinnacher, R. M.; Begg, J. D.; Mason, H.; Ranville, J.; Powell, B. A.; Wong, J. C.; Kersting, A. B.; Zavarin, M., Effect of Fulvic Acid Surface Coatings on Plutonium Sorption and Desorption Kinetics on Goethite. *Environmental Science & Technology* **2015,** *49*, (5), 2776-2785.

27. Kaplan, D. I.; Powell, B. A.; Gumapas, L.; Coates, J. T.; Fjeld, R. A.; Diprete, D. P., Influence of pH on plutonium desorption/solubilization from sediment. *Environmental Science & Technology* **2006,** *40*, (19), 5937-5942.

28. Begg, J. D.; Zavarin, M.; Kersting, A. B., Desorption of plutonium from montmorillonite: An experimental and modeling study. *Geochimica Et Cosmochimica Acta* **2017,** *197*, 278-293.

29. Begg, J. D.; Zavarin, M.; Tumey, S. J.; Kersting, A. B., Plutonium sorption and desorption behavior on bentonite. *J. Environ. Radioact.* **2015,** *141*, 106-114.

30. Begg, J. D.; Zavarin, M.; Kersting, A. B., Plutonium Desorption from Mineral Surfaces at Environmental Concentrations of Hydrogen Peroxide. *Environmental science & technology* **2014,** *48*, (11), 6201-6210.

31. Begg, J. D.; Zavarin, M.; Zhao, P.; Tumey, S. J.; Powell, B.; Kersting, A. B., Pu(V) and Pu(IV) sorption to montmorillonite. *Environ. Sci. Technol.* **2013,** *47*, (10), 5146-5153.

32. Tinnacher, R. M.; Zavarin, M.; Powell, B. A.; Kersting, A. B., Kinetics of neptunium(V) sorption and desorption on goethite: An experimental and modeling study. *Geochim. Cosmochim. Acta* **2011,** *75*, (21), 6584-6599.

33. Parkhurst, D. L.; Appelo, C. A. J., Description of input and examples for PHREEQC version 3 - A computer program for speciation, batch-reaction, one-dimensional transport, and inverse geochemical calculations. In *Techniques and Methods, Book 6*, USGS: Denver, CO, 2012; p 497.

34. Giffaut, E.; Grivé, M.; Blanc, P.; Vieillard, P.; Colàs, E.; Gailhanou, H.; Gaboreau, S.; Marty, N.; Madé, B.; Duro, L., Andra thermodynamic database for performance assessment: ThermoChimie. *Appl. Geochem.* **2014,** *49*, (Supplement C), 225-236.

35. Grivé, M.; Duro, L.; Colàs, E.; Giffaut, E., Thermodynamic data selection applied to radionuclides and chemotoxic elements: An overview of the ThermoChimie-TDB. *Appl. Geochem.* **2015,** *55*, (Supplement C), 85-94.

36. Doherty, J., PEST Model-Independent Parameter Estimation. In Watermark Numerical Computing: 2004.

37. Reynolds, M., *X-Ray Diffraction and the Identification and Analysis of Clay Minerals, 2nd ed. xviii + 378 pp. Oxford, New York: Oxford University Press. Price £27.95 (spiral-bound paperback). ISBN 0 19 508713 5*. 1998/11/01 ed.; Cambridge University Press: 1997; Vol. 135, p 819-842.

38. Inoue, A.; Utada, M.; Wakita, K., Smectite-to-illite conversion in natural hydrothermal systems. *Applied Clay Science* **1992,** *7*, (1), 131-145.

39. Meunier, A.; Velde, B.; Griffault, L., The reactivity of bentonites: a review. An application to clay barrier stability for nuclear waste storage. *Clay Minerals* **1998,** *33*, (2), 187-196.

40. Beaufort, D.; Berger, G.; Lacharpagne, J. C.; Meunier, A., An experimental alteration of montmorillonite to a di plus trioctahedral smectite assemblage at 100 and 200 degrees C. *Clay Minerals* **2001,** *36*, (2), 211-225.

41. Hawkins, D. B., Kinetics of Glass Dissolution and Zeolite Formation under Hydrothermal Conditions. *Clays and Clay Minerals* **1981,** *29*, (5), 331-340.

42. Zhao, P.; Tinnacher, R. M.; Zavarin, M.; Kersting, A. B., Analysis of trace neptunium in the vicinity of underground nuclear tests at the Nevada National Security Site. *Journal of Environmental Radioactivity* **2014,** *137*, 163-172.

43. Liu, L. Y.; Shen, L.; Li, W. R.; Min, F. F.; Lu, F. Q., Study on the aggregation behavior of kaolinite particles in the presence of cationic, anionic and non-ionic surfactants. *Plos One* **2018,** *13*, (9), 15.

44. Oliveira, C. d. R.; Rubio, J., Adsorption of ions onto treated natural zeolite. *Materials Research* **2007,** *10*, 407-412.

45. Li, Z.; Alessi, D.; Allen, L., Influence of quaternary ammonium on sorption of selected metal cations onto clinoptilolite zeolite. *J. Environ. Qual.* **2002,** *31*, (4), 1106-1114.

46. Siroux, B.; Beaucaire, C.; Tabarant, M.; Benedetti, M. F.; Reiller, P. E., Adsorption of strontium and caesium onto an Na-MX80 bentonite: Experiments and building of a coherent thermodynamic modelling. *Applied Geochemistry* **2017,** *87*, (Supplement C), 167-175.

47. Zhao, P. H.; Begg, J. D.; Zavarin, M.; Tumey, S. J.; Williams, R.; Dai, Z. R. R.; Kips, R.; Kersting, A. B., Plutonium(IV) and (V) Sorption to Goethite at Sub-Femtomolar to Micromolar Concentrations: Redox Transformations and Surface Precipitation. *Environmental Science & Technology* **2016,** *50*, (13), 6948-6956.

48. Sanchez, A. L.; Murray, J. W.; Sibley, T. H., The adsorption of plutonium IV and V on goethite. *Geochimica et Cosmochimica Acta* **1985,** *49*, (11), 2297-2307.

LLNL-JRNL-764142

49. Banik, N. L.; Marsac, R.; Lutzenkirchen, J.; Diascorn, A.; Bender, K.; Marquardt, C. M.; Geckeis, H., Sorption and Redox Speciation of Plutonium at the Illite Surface. *Environmental Science & Technology* **2016,** *50*, (4), 2092-2098.

50. Hu, Q.; Zavarin, M.; Rose, T., Effect of reducing groundwater on the retardation of redox-sensitive radionuclides. *Geochem. Trans.* **2008,** *9*, (1), 12.